Chaos, Solitons and Fractals 42 (2009) 2047–2056

Contents lists available at ScienceDirect

Chaos, Solitons and Fractals

journal homepage: www.elsevier.com/locate/chaos

Fractal analysis of damage detected in concrete structural elements under loading

A. Carpinteri *, G. Lacidogna, G. Niccolini

Politecnico di Torino, Department of Structural Engineering and Geotechnics, Corso Duca degli Abruzzi 24, 10129 Torino, Italy

ARTICLE INFO

Article history:
Accepted 30 March 2009

ABSTRACT

In Civil Engineering materials subjected to stress or strain states a quantitative evaluation of damage is of great importance due to the critical character of this phenomenon, which at a certain point suddenly turns into a catastrophic failure. An effective damage assessment criterion is represented by the statistical analysis of the amplitude distribution of acoustic emission (AE) signals emerging from the growing microcracks. The amplitudes of such signals are distributed according to the Gutenberg–Richter (GR) law and characterised through the *b*-value which decreases systematically with damage growth. On the other hand, the damage process is also characterised by the progressive coalescence of microcracks to form fracture surfaces. Geometrically the fractal dimension *D* of the damaged domain is expected to decrease from an initial value comprised between 2 and 3 towards a final value nearly equal to 2. The *b*-value and the fractal analysis, are here applied to two case studies of concrete specimens loaded up to failure, and the obtained results are compared and discussed. In particular, we emphasize that a single fractal dimension does not adequately describe a crack network, since two damaged domains with the same fractal dimension could have significantly different properties.

1. Introduction

The demands for assuring the safety and the performance in Civil Engineering requires as non-invasive as possible inspections in order to estimate the physical conditions of in-service structures. The phenomenon of damage from a physical point of view represents surface discontinuities in the form of cracks, or volume discontinuities in the form of cavities [1,2]. It is very difficult to macroscopically distinguish a highly damaged volume element from an undamaged one since the depth of cracks or interior defects cannot be identified. It therefore becomes necessary to imagine internal variables representative of the deteriorated state of the material which are directly accessible to measurement [1–3].

The most advanced method of quantitative non-destructive evaluation of damage progression is the acoustic emission (AE) technique. Technically, the expression "acoustic emission" (AE) is used to mean a class of phenomena in which transient elastic waves are generated by the rapid release of energy from localised sources, typically developing cracks, within a material. AE waves, whose frequencies typically range from kHz to MHz, propagate through the material towards the surface of the structural element, where they can be detected by sensors which turn the released strain energy packages into electrical signals [4–13]. A typical AE sensor transforms elastic vibrations, i.e. stress waves, of 10^{-9} mm amplitude into electric signals of 10 μV amplitude. In the presented case studies, USAM® resonant sensors (accepting signals in the range between 50 and 800 kHz) have been used, since concrete attenuates emission strongly and maximum sensitivity was required [9,10,12].

Traditionally, in AE testing a number of parameters are recorded from the signals. The condition of the specimen is determined from these parameters. Important parameters include the arrival time and the amplitude. Another main step of the AE

* Corresponding author.
E-mail address: alberto.carpinteri@polito.it (A. Carpinteri).

0960-0779/$ - see front matter © 2009 Elsevier Ltd. All rights reserved.
doi:10.1016/j.chaos.2009.03.165

analysis is the location of AE sources due to developing microcracks inside the specimen volume. Several authors have worked on the source location of acoustic emissions using triangulation techniques similar to the determination of earthquake hypocentres [14–16]. The triangulation process requires the solution of a system of simultaneous equations containing the measured arrival time differences at different sensors of the AE waves.

Using AE technique an effective damage assessment criterion is represented by the statistical analysis of the amplitude distribution of AE signals emerging from the growing microcracks. The amplitudes of such signals are distributed according to the Gutenberg–Richter (GR) law, $N\ (\geqslant A) \propto A^{-b}$, where N is the number of AE signals with amplitude $\geqslant A$. The exponent b of the GR law, the so-called b-value, changes with the different stages of damage growth: the initially dominant microcracking generates a large number of low-amplitude AE signals, while the following macrocracking generates less signals but of higher amplitude. This implies a progressive decrease of the b-value as the specimen approaches impending failure: this is the core of the so-called "b-value analysis" used for damage assessment [4–10,12,17].

On the other hand, the damage process is also characterised by its progressive localization: at its early stage, damage consists of a myriad of microcracks chaotically distributed over a large part of the specimen volume, whereas at the final stage microcracks coalesce to form the through-going fracture surface. In geometric words, the fractal dimension D of the damaged domain is expected to decrease from an initial value comprised between 2 and 3 towards a final value nearly equal to 2 [10–12]. Therefore, both parameters b and D share a decreasing trend as the damage develops and then have the potential for monitoring the damage progression.

The presented methods of damage assessment, the b-value and the fractal analysis, are here applied to two case studies of concrete specimens monitored by AE sensors and loaded up to failure. In particular, we emphasize that a single fractal dimension does not adequately describe a crack network, since two damaged domains with the same fractal dimension could have significantly different properties.

2. The *b*-value analysis

Magnitude (m) is a log scale coming from Geophysics often used to measure the amplitude of a measured electrical signal generated by an AE event. The magnitude is related to the amplitude A expressed in microvolts (μV) by the equation [4,6,9,10,17]:

$$m = \mathrm{Log}_{10} A. \tag{1}$$

It is widely accepted the Gutenberg–Richter (GR) law, initially drawn in seismicity, which describes the statistical distribution of AE signal amplitudes [4,6,9,10,17]:

$$\mathrm{Log}N\ (\geqslant m) = a - bm, \tag{2}$$

where N is the number of signals with magnitude greater than m, while the coefficient b, called "b-value", is the negative slope of Log$N$ vs. m diagram. Microcracks release low-amplitude AEs, while macrocracks release high-amplitude AEs. This intuitive relation is confirmed by the experimental result that the area of a crack advancement is proportional to the amplitude of related AE signal [13].

From Eq. (2) it turns out that a regime of microcracking generates weak AEs, and therefore leads to relatively high b-values (raising the threshold m, the number of surviving signals rapidly decays). When macrocracks start to appear, instead, lower b-values are observed.

Therefore the analysis of b-value, which changes systematically with the different stages of fracture process [4–10,12,17], has been recognised as a useful tool for damage level assessment. In general terms, the fracture process moves from micro to macrocracking as the material approaches impending failure and the b-value decreases. While testing the materials undergoing brittle failure, the b-value is found to range from 1.5 to 2.5 in the initial stages. It then decreases with increase in stress to attain values $\approx$1 and less as the failure approaches in the material [6,7,9,10,12,17].

Furthermore, as pointed out in [17], the b-value statistical analysis is in close connection with the fractal geometry approach in the mechanics of damage and fracture of heterogeneous materials. Fractal geometry represents the natural tool to characterise self-organised processes, emphasizing their universality and the scaling laws arising at the critical points. Among the results obtained by the senior author, we could cite the modelling of the size-scale effects on strength, toughness [18–20] and critical strain [21] of heterogeneous materials and the optimization of the mechanical properties of advanced materials [22]. Further results include the development of an original fractional calculus-based framework for the analysis of materials with complex damage occurring in fractal domains [23] and the modelling of the scaling laws for fatigue [24] and friction [25]. Eventually, it is worthwhile recalling that the fractal geometry approach, together with Renormalization Group theory, has found an application also in seismology [26], that is a field with strong analogies to material damage and fracture.

3. Measuring the fractal dimension of a damaged domain

Fractal geometry has been widely used for the description of irregular phenomena in various scientific fields recently. As already remarked in the characterization of fracture systems, fractals are used to represent damaged domains, i.e. microcrack networks [10–12,17,27–30] and fracture surfaces [18,31], even at geological scale [26], and disordered materials in general [21].

The fractal dimension D of a set S of points (point here stands for microcrack) is the critical value D of the exponent δ for which the measure M_δ of S changes from zero to infinity [32]:

$$M_\delta = N(d)d^\delta \underset{d\to 0}{\to} \begin{cases} 0, & \delta > D, \\ \infty, & \delta < D, \end{cases} \tag{3}$$

where $N(d)$ is the number of boxes of characteristic length scale d needed to cover S (in the case of a smooth surface shown in Fig. 1, applying Eq. (3) correctly gives $D = 2$).

Starting from the definition of Eq. (3), the operative method to determine the fractal dimension D in nontrivial cases is counting the number $N(d)$ of boxes needed to cover S for different values of d. As it follows from Eq. (3), asymptotically, in the limit of small d, we have [32]:

$$N(d) \propto d^{-D}. \tag{4}$$

The fractal dimension D, called *box-counting dimension*, is determined from Eq. (4) by finding the slope of $\ln N(d)$ plotted vs. $\ln d$.

The box-counting method allows a generalization to the concept of multifractality. For each d, the box-counting method ignores irregularities of size less than d, since the number of points found inside the boxes that intersect the set is not relevant [32]: a box containing one crack of the network and another containing 100 cracks count the same (Fig. 2a). Therefore, the sole knowledge of the box-counting dimension D is thus not sufficient to fully characterise the fractal geometry of a microcrack network [28,33], since two crack networks with the same D could have significantly different distributions of crack density [34], while the box-counting dimension D only provides global (or average) information of a crack network ignoring local irregularities [35].

In order to develop a multifractal model, each covering box is weighted by the number of cracks inside it divided by the total number of cracks in the body (Fig. 2b), $\mu_i = n_i/N_{TOT} < 1$ (note that this is not the only possible choice, since μ_i could be the total crack length L_i in the ith box [28]).

The generalised fractal dimension D_q of a crack network is introduced in the following way [28,32]:

$$D_q \equiv \frac{1}{(q-1)} \lim_{d\to o} \frac{\ln \sum \mu_i^q}{\ln d}, \quad \forall q \in \Re. \tag{5}$$

Note that $D_q = 0$ is the box-counting dimension D. A fractal network is characterised by an infinite set of generalised dimensions D_q for all real q values, called the multifractal spectrum [28,32,33]. Since $\mu_i < 1$, it follows that $\mu_i^0 > \mu_i > \mu_i^2 > \cdots$, and then $D_0 > D_1 > D_2 > \cdots$. The equalities between generalised dimensions, $D_0 = D_1 = D_2 = \cdots$, hold only for uniform crack

Fig. 1. A smooth surface S is measured by counting the number $N(d)$ of squares of characteristic length scale d needed to cover it. Referring to Eq. (3), the measure is the area $A = N(d)d^2$, for $d \to 0$. Trying to measure the volume of S we obtain a vanishing value; $V = N(d)d^3 = Ad \to 0$ for $d \to 0$, while the length diverges, $L = N(d)d = Ad^{-1} \to \infty$ for $d \to 0$.

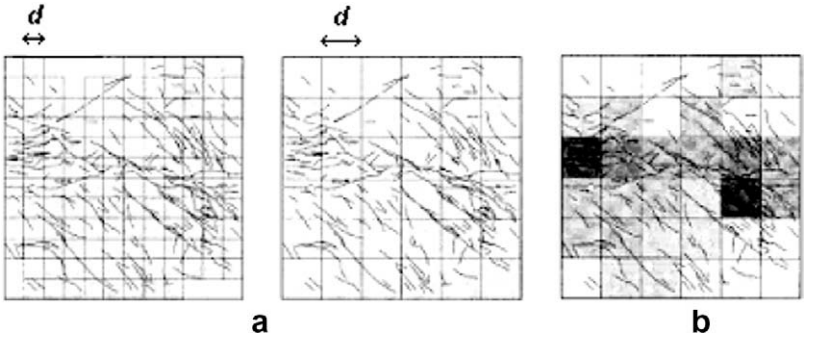

Fig. 2. Classical methods used to calculate the fractal dimension of a microcrack network. The box-counting method equally counts boxes provided that they contain at least one crack (a); the multifractal analysis weights each box by its crack content. The darker the box, the more numerous the cracks found inside it (b).

densities ($\mu_i = d^3$). As shown in [32], we can check the correctness of this statement in the case of a uniform crack distribution in a three-dimensional domain, dividing this space into $N = d^{-3}$ boxes with a volume of d^3 each. Then the probability μ_i of finding one crack in the ith box is proportional to its volume, $\mu_i = d^3$, and we find:

$$\sum_{i=1}^{N} \mu_i^q = \sum_{i=1}^{N} d^{3q} = d^{3(q-1)}. \tag{6}$$

Inserting Eq. (6) into Eq. (5) gives:

$$D_q = \frac{1}{q-1} \lim_{d \to o} \frac{\ln d^{3(q-1)}}{\ln d} = 3, \quad \forall q, \tag{7}$$

which is the expected dimension of a damaged volume uniformly filled with cracks, proving thus also the consistency of the generalised definition of fractal dimension given in Eq. (5).

On the contrary, multifractality (i.e., monotone decreasing fractal dimensions D_q for increasing q) reflects non-uniformity crack density: the greater the differences $(D_0 - D_q)$, the less uniform the crack distribution. The easiest generalised fractal dimension to estimate is the *correlation dimension* $(D_{q=2})$. Therefore, crack networks which tend to cluster will be characterised by lower values of D_2 than uniform crack densities, giving thus $D_2 < D_0$, while for uniform crack densities $D_2 = D_0$, as proved in Eq. (7). In other words, the greater the difference $(D_0 - D_2)$, the stronger the spatial clustering or the non-uniformity of a crack network [34,35].

Since μ_i represents the probability of finding one crack in the ith box, then μ_i^2 is the probability of finding two cracks in this box, and $\sum \mu_i^2$ is the probability of finding two cracks in the same box, whatever is. The easiest algorithm to estimate $\sum \mu_i^2$ is the two-point correlation function [12,28,36]:

$$C(d) \equiv \frac{2}{N(N-1)} \sum_{k=1}^{N-1} \sum_{j=k+1}^{N} \Theta(d - \|\mathbf{x}_k - \mathbf{x}_j\|), \tag{8}$$

where N is the total number of cracks, the double sum counts the number of pairs of cracks whose distance apart is less than d, divided by the total number of pairs which is possible to form with N cracks, and $\Theta(x)$ is the Heaviside step function (equal to 1 if $x > 0$, and zero otherwise).

In fact, taking an arbitrary crack in $\mathbf{x}_i$, $C(d)$ gives thus the probability of finding another one in the sphere of radius d centred at $\mathbf{x}_i$, which is nearly equal to the probability of finding two cracks in a cube with edge d:

$$\sum_i \mu_i^2 \cong C(d). \tag{9}$$

Therefore, Grassberger and Procaccia [36] suggested an easy way of calculating the correlation dimension $D_{q=2}$ by means of the two-point correlation function:

$$D_2 = \lim_{d \to o} \frac{\ln \sum_i \mu_i^2}{\ln d} \cong \lim_{d \to o} \frac{\ln C(d)}{\ln d}. \tag{10}$$

When $C(d)$ exhibits a power-law behaviour, $C(d) \propto d^{D2}$, the exponent D_2 is the correlation dimension of the crack network.

4. Three-point bending test

In order to determine the fracture process zone in a specimen subject to a three-point bending test, the acoustic emissions emerging from growing microcracks were monitored. The specimen was a prism measuring $8 \times 15 \times 70$ cm^3, with a central 5 cm notch cut into it beforehand to ensure a central crack, and with a fiber content of 40 kg/m^3 for a resulting Young's modulus of 35 GPa. The test was performed in displacement control by imposing a constant displacement rate equal to 10^{-3} mm/s.

Five AE transducers were fitted to the specimen at points shown in Fig. 3a. During the loading test, the AE source location procedure was successfully applied to identify the fracture process zone. In this way, AE clusters are seen to propagate with increasing load, following satisfactorily the growth of the central crack (see again Fig. 3a). The load vs. time curve for the specimen, with its softening branch characterizing the AE activity, is shown in Fig. 3b.

In order to investigate the behaviour of the specimen by means of the b-value analysis, the load–time diagram was broken down into three stages: a first stage (t_0, t_1) extending from the initial time to peak load, a second stage (t_1, t_2) going from peak load to the peak of AE activity, or mainshock, and a third stage (t_2, t_f) going from the mainshock to the end of the process. The b-values are shown for each stage in Fig. 3c: they exhibited a decreasing trend as the specimen approached the impending failure, ranging from 1.49 to 1.11. The minimum value is obtained in the softening branch of the load–time curve, and it is very close to the lower limit 1, theoretically predicted by Carpinteri et al. [9,10,12,17], to the b-values observed in most of specimens tested up to the failure. Therefore, we calculated the fractal dimension of the damaged domain, represented by the crack network located by AE technique, using both the box-counting method and the two-point correlation algorithm. In both cases, we have calculated the fractal dimension at two different stages of the damage process, considering

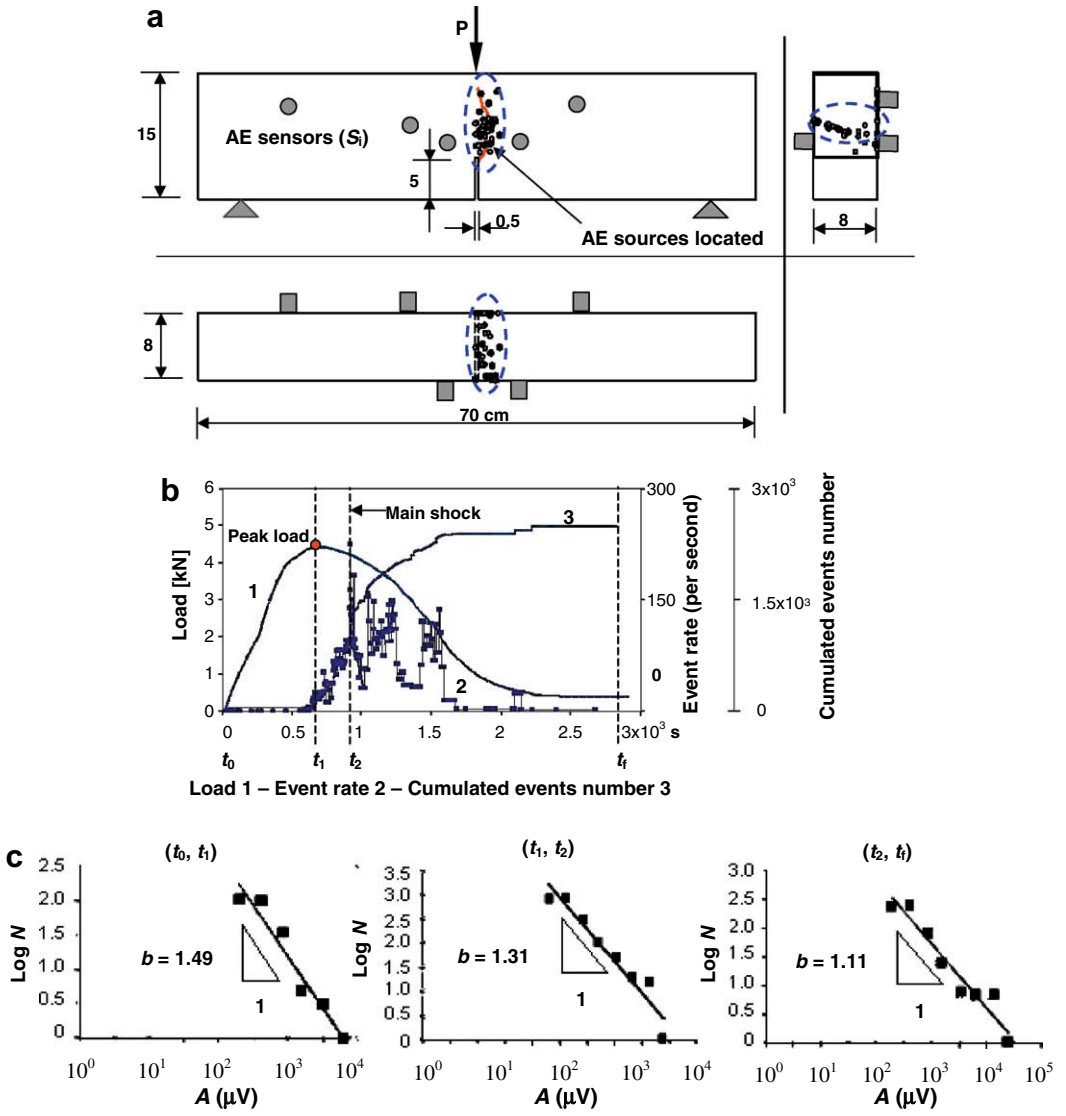

Fig. 3. Three bending point test. (a) The localised crack points identifying the fracture process zone in a narrow band. (b) Load vs. time curve and AE activity. (c) *b*-values during the loading test.

the previous partition; the first stage (t_0, t_1) has not been considered, due to insufficient number of localized points for fractal analysis.

The box-counting dimension D_0 reached the value of 2.17 in the intermediate stage (t_1, t_2), and 2.04 in the final stage (t_2, t_f), while the correlation dimension D_2 was respectively 1.21 and 1.17 (see Fig. 4a and b). The nearly constant values exhibited at different stages by D_0 suggest that, since the beginning, damage concentrated over the central crack, as confirmed by visual inspection, which progressively opened up to failure. On the other hand, the great difference $(D_0 - D_2)$ constitutes a measure of the high degree of damage localization in a narrow band due to the presence of the central notch [34].

5. Concrete specimen in compression

As a second case study, the behaviour of a concrete specimen in compression during a laboratory test has been investigated through AE monitoring. Six AE transducers (S_{AE}) have been applied to the surface of the specimen, a prism measuring $160 \times 160 \times 500\ \text{mm}^3$ (Fig. 5).

The test has been performed in displacement control by an electronic controlled Servo-hydraulic Material Testing Systems machine (311,31 model) with a capacity of 1800 kN, imposing a constant rate of displacement to the upper loading platen: in the first 10^4 s the displacement rate was $\mathrm{d}\delta/\mathrm{d}t = 10^{-5}$ mm/s, increased to 10^{-4} mm/s from $t = 10^4$ s up to failure.

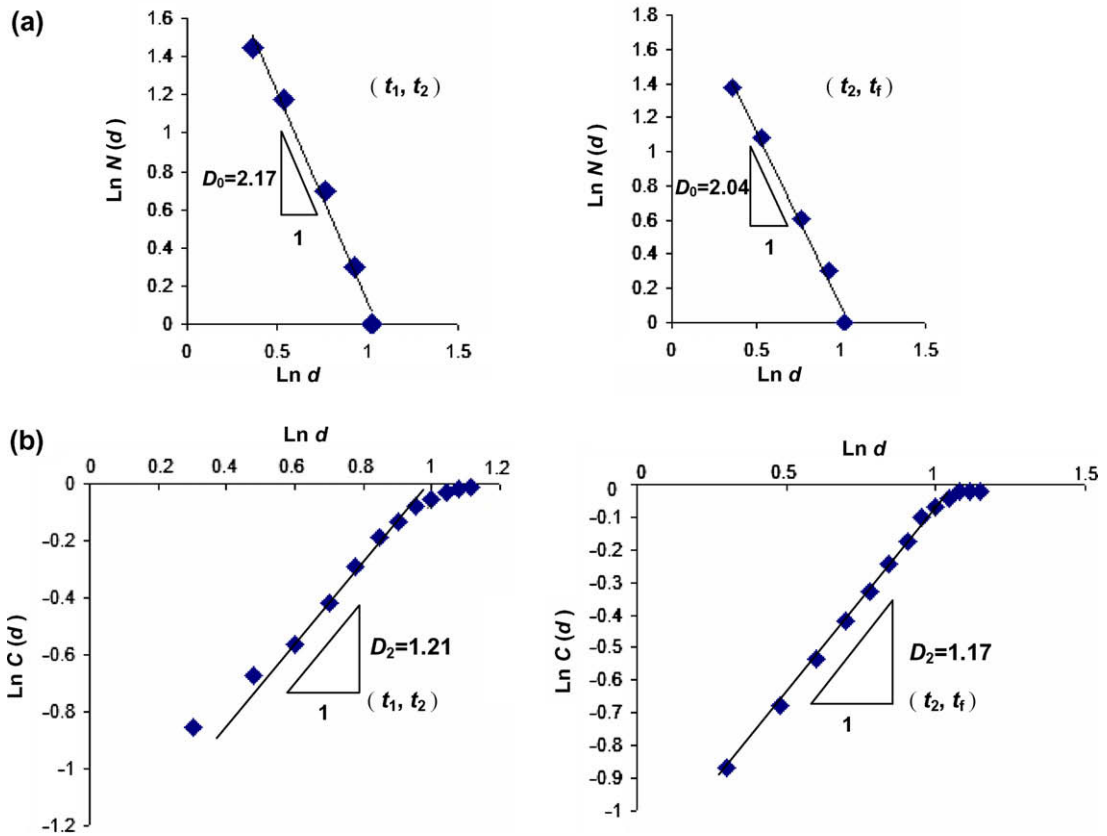

Fig. 4. Fractal dimension evolution of damaged region by means of the box-counting method (a) and the two-point correlation function (b). d (cm) is the size of the covering regular mesh.

This kind of machine is controlled by an electronic closed-loop servo-hydraulic system (Fig. 6b). It is therefore possible to perform tests under load or displacement control. The displacements are recorded by four strain gauges (HBM 1-LY41-50/120 model) applied on the specimen surface. In spite of the low value chosen for the displacement rate, the specimen has failed in a brittle manner as it can be seen in the load vs. time (strain) diagram of Fig. 6a, where the linear branch extends over almost the entire duration of the test.

Even in this case, the characterization of the fracture process has been carried out using the b-value analysis and the fractal analysis. We partitioned the loading test in three stages: the first stage, where linear elasticity was still applicable, and two following stages characterised by deviations from linear elasticity and existence of damage. The b-value calculated at the earliest stage of the loading test, where linear elasticity was still applicable, gives 1.75, index of low damage level. The b-values calculated in the two following stages of the damage region, give respectively 1.39 and 1.26, confirming the decreasing trend of b-value as the damage develops (Fig. 7).

The same temporal partition used for the b-value analysis has been used for the fractal analysis. In the linear regime, the recorded low-amplitude AE signals have not allowed the location of microcracks (an AE event must be detected by at least two transducers for crack location), then neither the calculation of fractal dimensions. We calculated the box-counting dimension D_0 and the correlation dimension D_2 at the two different stages of the damage region.

The box-counting dimension D_0 reached the value of 2.21 at earlier stage of the damage region and then decreased to 2.10 at the final stage of the test (Fig. 8). At the same stages, the correlation dimension D_2 respectively reached the values of 2.20 and 1.91 (Fig. 9). In this second case study, the difference $(D_0 - D_2)$ is smaller than in the three-point bending test, indicating a more homogeneous distribution of the microcracks throughout the specimen volume, as can be visually appreciated from Fig. 10 as well, where the localised AE crack sources are overlapped to the fracture surface.

In absence of pre-existing crack or notch which concentrate the applied stress, a progressive localization of damage, captured by the decreasing trend exhibited by both D_0, has been observed: damage evolves from microcracks trying to fill up the specimen volume to microcracks mainly localised on the through-going fracture surface. Looking at the gentle decrease of D_0 (going from 2.21 to 2.10), the progressive localization of damage is not marked, reflecting a brittle response of the specimen, as moreover illustrated by the load–displacement curve of Fig. 6a. Recall that a response will be referred to as being brittle if it is dominated by few large cracks.

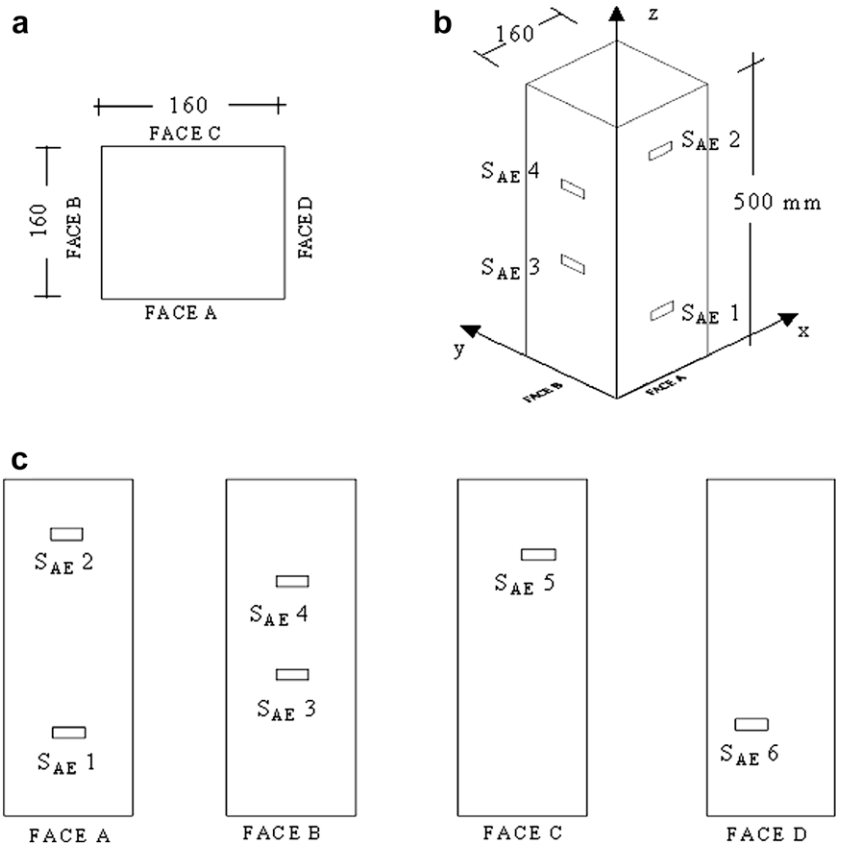

Fig. 5. Concrete specimen in compression. (a) Cross-section of the specimen. (b) Assonometric projection with the positioned AE sensors. (c) Overview of the four specimen faces.

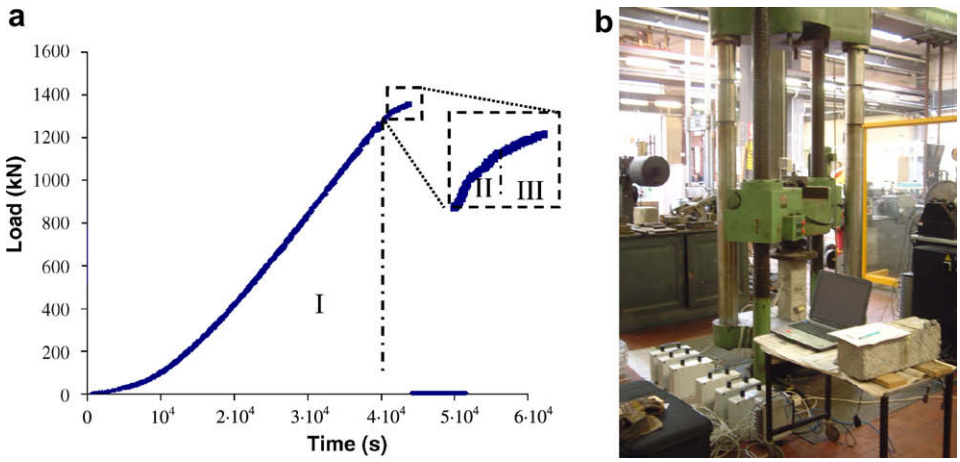

Fig. 6. Concrete specimen in compression. (a) Load–time diagram of the test performed in displacement control. The specimen failed in a quasi-brittle manner: in region I, where linear elasticity is applicable, there is little damage (i.e., low-amplitude AE events), while in regions II and III, damage results in a deviation from linear elasticity and an increase of AE level. (b) Photo of MTS machine and of the specimen during the test. Note on the left the devices utilized for detection of AE signals.

6. Conclusions

Two approaches based on the AE technique for assessing the level and the degree of localization reached by the damage in concrete structures are shown. The first one, called *b*-value analysis, has been applied to the two considered case studies, confirming its reliability for predicting impending failures, i.e. *b*-value tending to 1 at the rupture. The second approach is

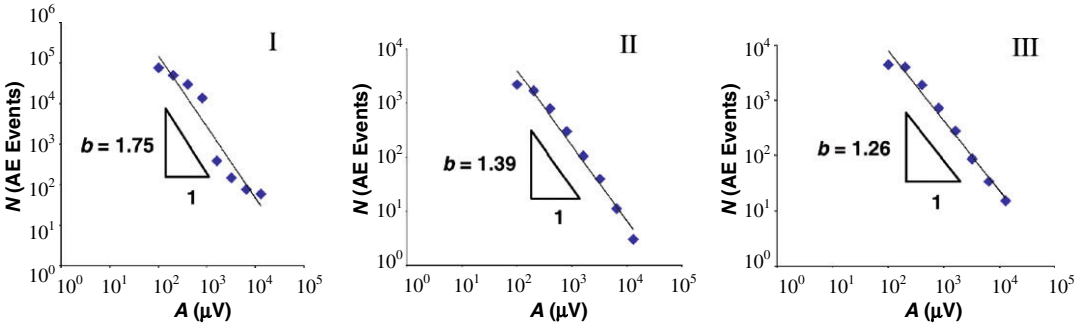

Fig. 7. Concrete specimen in compression: *b*-values during the three stages of the loading test. Note that the event amplitudes *A* instead of the magnitudes *m* are reported in the *x*-axis.

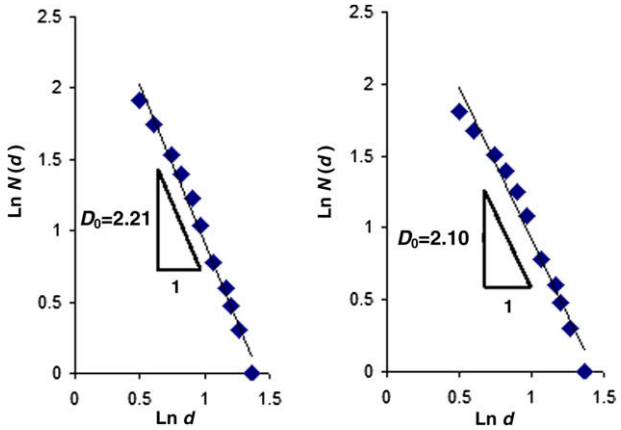

Fig. 8. Evolution of damaged region dimension from the intermediate stage (stage II) to the final stage (stage III) by means of the box-counting method. *d* (cm) is the size of the covering regular mesh.

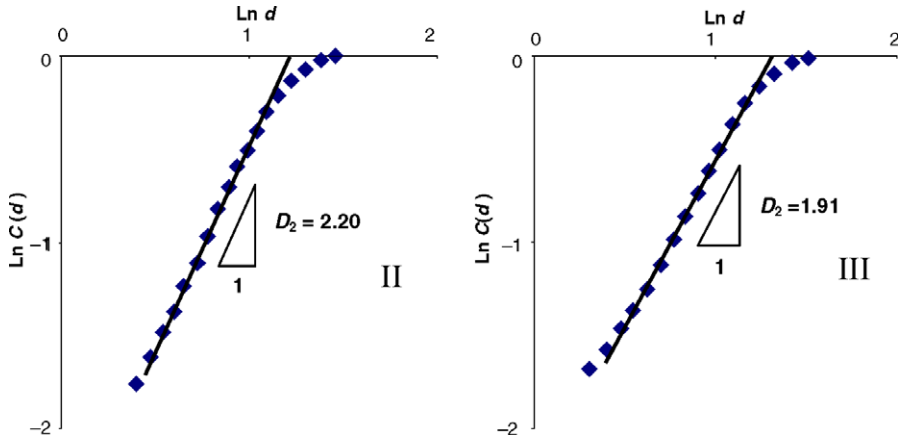

Fig. 9. Evolution of damaged region dimension from the intermediate stage (stage II) to the final stage (stage III) by means of the two-point correlation function.

a fractal analysis of the damage domain, which has been applied to the same case studies. The box-counting dimension D_0 provides global, or average, information of the damaged domain but is not able to distinguish between the crack networks of two presented case studies, characterised by different degrees of heterogeneity. The difference $(D_0 - D_2)$ constitutes a measure of the degree of heterogeneity, proving to be a useful tool for emphasizing the existence of spatial clustering of cracks.

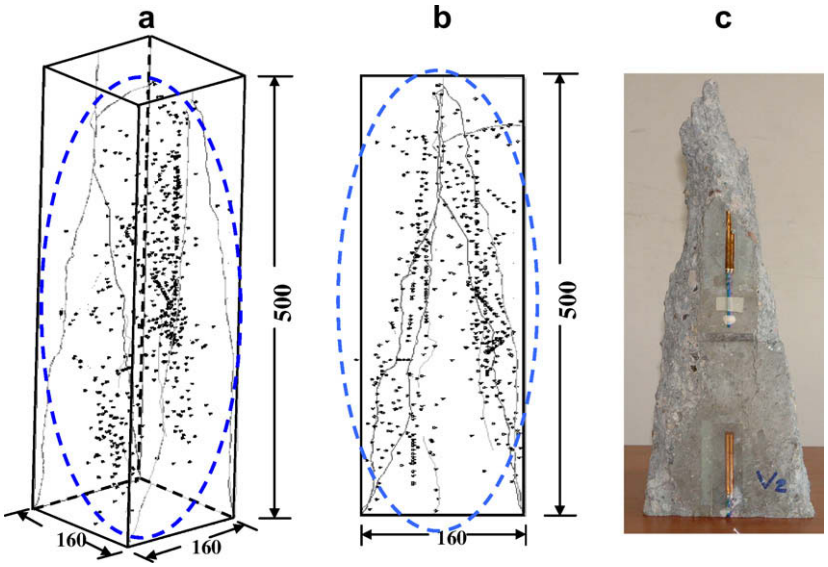

Fig. 10. (a) Final overview of the localized AE crack sources overlapped to the fracture surfaces. (b) Projections of the AE sources and fracture surfaces identified during the loading test (the dimensions are expressed in mm). (c) Broken specimen after testing.

Acknowledgement

The financial support provided by the European Union to the Leonardo da Vinci ILTOF Project (Innovative Learning and Training on Fracture) is gratefully acknowledged.

References

[1] Lemaitre J, Chaboche JL. Mechanics of solid materials. Cambridge: University Press; 1990.
[2] Krajcinovic D. Damage mechanics. Elsevier; 1996.
[3] Turcotte DL, Newman WI, Shcherbakov R. Micro and macroscopic models of rock fracture. Geophys J Int 2003;152:718–28.
[4] Shiotani T, Fujii K, Aoki T, Amou K. Evaluation of progressive failure using AE sources and improved *b*-value on slope model tests. Prog Acoust Emission VII 1994;7:529–34.
[5] Ohtsu M. The history and development of acoustic emission in concrete engineering. Mag Concr Res 1996;48:321–30.
[6] Colombo S, Main IG, Forde MC. Assessing damage of reinforced concrete beam using "*b*-value" analysis of acoustic emission signals. J Mater Civil Eng, ASCE 2003;15:280–6.
[7] Rao MVMS, Lakshmi KJP. Analysis of *b*-value and improved *b*-value of acoustic emissions accompanying rock fracture. Curr Sci 2005;89:1577–82.
[8] Kurz JH, Finck F, Grosse CU, Reinhardt HW. Stress drop and stress redistribution in concrete quantified over time by the *b*-value analysis. Struct Health Monitor 2006;5:69–81.
[9] Carpinteri A, Lacidogna G, Niccolini G. Critical behaviour in concrete structures and damage localization by acoustic emission. Key Eng Mater 2006;312:305–10.
[10] Carpinteri A, Lacidogna G, Niccolini G, Puzzi S. Critical defect size distributions in concrete structures detected by the acoustic emission technique. Meccanica 2008;43:349–63.
[11] Lu C, Mai YW, Xie H. A sudden drop of fractal dimension: a likely precursor of catastrophic failure in disordered media. Philos Mag Lett 2005;85:33–40.
[12] Carpinteri A, Lacidogna G, Niccolini G, Puzzi S. Morphological fractal dimension versus power-law exponent in the scaling of damaged media. Int J Damage Mech 2009;18:259–82.
[13] Pollock AA. Acoustic emission-2: acoustic emission amplitudes. Non-Destruct Test 1973;6:264–9.
[14] Grosse CU, Reinhardt HW, Dahm T. Localization and classification of fracture types in concrete with quantitative acoustic emission measurement techniques. NDT Int 1997;30:223–30.
[15] Shah SP, Li Z. Localisation of microcracking in concrete under uniaxial tension. ACI Mater J 1994;91:372–81.
[16] Carpinteri A, Lacidogna G, Niccolini G. Crack localisation in a large-sized R.C. beam through the acoustic emission technique. In: Proceedings of the 17th congress of theoretical and applied mechanics (AIMETA), Florence, Italy; 2005 [CD-Rom, Paper No. 23].
[17] Carpinteri A, Lacidogna G, Puzzi S. From criticality to final collapse: evolution of the *b*-value from 1.5 to 1.0. Chaos Soliton Fract 2009;41:843–53.
[18] Carpinteri A. Scaling laws and renormalization groups for strength and toughness of disordered materials. Int J Solid Struct 1994;31:291–302.
[19] Carpinteri A, Chiaia B. Power scaling laws and dimensional transitions in solid mechanics. Chaos Soliton Fract 1996;7:1343–64.
[20] Carpinteri A, Chiaia B. Multifractal scaling laws in the breaking behavior of disordered materials. Chaos Soliton Fract 1997;8:135–50.
[21] Carpinteri A, Cornetti P. A fractional calculus approach to the description of stress and strain localization in fractal media. Chaos Soliton Fract 2002;13:85–94.
[22] Carpinteri A, Pugno N, Puzzi S. Strength vs. toughness optimization of microstructured composites. Chaos Soliton Fract 2009;39:1210–23.
[23] Carpinteri A, Cornetti P, Kolwankar KM. Calculation of the tensile and flexural strength of disordered materials using fractional calculus. Chaos Soliton Fract 2004;21:623–32.
[24] Paggi M, Carpinteri A. Fractal and multifractal approaches for the analysis of crack-size dependent scaling laws in fatigue. Chaos Soliton Fract 2009;40:1136–45.
[25] Carpinteri A, Paggi M. A fractal interpretation of size-scale effects on strength, friction and fracture energy of faults. Chaos Soliton Fract 2009;39:540–6.
[26] Carpinteri A, Chiaia B, Invernizzi S. Applications of fractal geometry and renormalization group to the italian seismic activity. Chaos Soliton Fract 2002;14:917–28.

[27] Bour O, Davy P. Clustering and size distributions of fault patterns: theory and measurements. Geophys Res Lett 1999;26:2001–4.
[28] Bonnet E, Bour O, Odling NE, Davy P, Main IG, Cowie P, et al. Scaling of fracture systems in geological media. Rev Geophys 2001;39:347–83.
[29] Carpinteri A, Pugno N. A fractal comminution approach to evaluate the drilling energy dissipation. Int J Numer Anal Method Geomech 2002;26:499–513.
[30] Carpinteri A, Lacidogna G, Pugno N. A fractal approach for damage detection in concrete and masonry structures by the acoustic emission technique. Acoust Tech 2004;38:31–7.
[31] Weyss J. Self-affinity of fracture surfaces and implications on a possible size effect on fracture energy. Int J Fract 2001;109:365–81.
[32] Feder J. Fractals. Plenum Press; 1988.
[33] Bour O, Davy P, Darcel C, Odling N. A statistical scaling model for fracture network geometry, with validation on a multiscale mapping of a joint network (Hornelen Basin, Norway). J Geophys Res 2002;107(B6):4/1–4/12.
[34] Lacidogna G, Niccolini G, Carpinteri A. Spatial characterization of damage through the acoustic emission technique. In: Proceedings of the 18th congress of theoretical and applied mechanics (AIMETA), Brescia, Italy; 2007 [CD-Rom]..
[35] Posadas A, Gimenez D, Bittelli M, Vaz C, Flury M. Multifractal characterization of soil particle-size distributions. Soil Sci Soc Am J 2001;65:1361–7.
[36] Grassberger P, Procaccia I. Characterization of strange attractors. Phys Rev Lett 1983;50:346–9.